ceramics

MDPI

Article

Process Development for Additive Manufacturing of Alumina Toughened Zirconia for 3D Structures by Means of Two-Photon Absorption Technique

Gerhard Hildebrand [1], Johanna C. Sänger [1,2], Uwe Schirmer [1], Willi Mantei [3], Yannick Dupuis [3], Ruth Houbertz [3,4] and Klaus Liefeith [1,*]

[1] Institute for Bioprocessing and Analytical Measurement Techniques e.V., Rosenhof, 37308 Heilbad Heiligenstadt, Germany; gerhard.hildebrand@iba-heiligenstadt.de (G.H.); johanna.saenger@bam.de (J.C.S.); uwe.schirmer@iba-heiligenstadt.de (U.S.)
[2] Bundesanstalt für Materialforschung und-Prüfung, Unter den Eichen 87, 12205 Berlin, Germany
[3] Multiphoton Optics GmbH, Friedrich-Bergius-Ring 15, 97076 Würzburg, Germany; willi.mantei@multiphoton.de (W.M.); yannick.dupuis@posteo.de (Y.D.); ruth.houbertz@thinkmade-consult.de (R.H.)
[4] ThinkMade Engineering & Consulting, Salvatorstrasse 17B, 97074 Würzburg, Germany
* Correspondence: klaus.liefeith@iba-heiligenstadt.de; Tel.: +49-3606-671-500

Abstract: Additive manufacturing is well established for plastics and metals, and it gets more and more implemented in a variety of industrial processes. Beside these well-established material platforms, additive manufacturing processes are highly interesting for ceramics, especially regarding resource conservation and for the production of complex three-dimensional shapes and structures with specific feature sizes in the µm and mm range with high accuracy. The usage of ceramics in 3D printing is, however, just at the beginning of a technical implementation in a continuously and fast rising field of research and development. The flexible fabrication of highly complex and precise 3D structures by means of light-induced photopolymerization that are difficult to realize using traditional ceramic fabrication methods such as casting and machining is of high importance. Generally, slurry-based ceramic 3D printing technologies involve liquid or semi-liquid polymeric systems dispersed with ceramic particles as feedstock (inks or pastes), depending on the solid loading and viscosity of the system. This paper includes all types of photo-curable polymer-ceramic-mixtures (feedstock), while demonstrating our own work on 3D printed alumina toughened zirconia based ceramic slurries with light induced polymerization on the basis of two-photon absorption (TPA) for the first time. As a proven exemplary on cuboids with varying edge length and double pyramids in the µm-range we state that real 3D micro-stereolithographic fabrication of ceramic products will be generally possible in the near future by means of TPA. This technology enables the fabrication of 3D structures with high accuracy in comparison to ceramic technologies that apply single-photon excitation. In sum, our work is intended to contribute to the fundamental development of this technology for the representation of oxide-ceramic components (proof-of-principle) and helps to exploit the high potential of additive processes in the field of bio-ceramics in the medium to long-term future.

Keywords: additive manufacturing; ceramics 3D printing; two-photon adsorption; polymer-ceramic mixtures; bio-ceramic engineering

Citation: Hildebrand, G.; Sänger, J.C.; Schirmer, U.; Mantei, W.; Dupuis, Y.; Houbertz, R.; Liefeith, K. Process Development for Additive Manufacturing of Alumina Toughened Zirconia for 3D Structures by Means of Two-Photon Absorption Technique. *Ceramics* **2021**, *4*, 224–239. https://doi.org/10.3390/ceramics4020017

Academic Editor: Gilbert Fantozzi

Received: 7 March 2021
Accepted: 7 May 2021
Published: 17 May 2021

1. Introduction

Highly complex technical ceramics are increasingly required in almost every field of application, including many industrial areas such as medical technology. Ceramics have a unique spectrum of electrical, optical, and magnetic properties as well as exceptional mechanical strength, thermal stability, hardness, and chemical resistance [1–3]. Additive manufacturing of ceramics has the potential to exceed the limitations of standard ceramic processing to open new fields of application while avoiding molding. Therefore, even in

small series, any application for complex shapes in the µm-up to the cm-range would be addressable [3].

In this context, several excellent reviews on additive manufacturing (AM) and 3D printing of ceramics have been recently published by e.g., Deckers et al. [4], Halloran et al. [5], and Chen et al. [6]. They all conclude that a variety of highly innovative technologies currently exists to additive fabrication to produce ceramic parts. All these currently existing 3D printing technologies for ceramics can be mainly divided into powder- and suspension-based technologies [2], while Chen et al. [6] also categorize bulk solid-based technologies separately.

Examples for powder-based procedures are 3D powder printing (3DP [3,7]), Laser Engineered Net Shaping (LENS^{TM} [8,9]), Selective Laser Sintering/Melting (SLS/SLM [10]), and Laminated Object Manufacturing (LOM [11]). A large variety of powder-based processes for ceramic production is reviewed by Deckers et al. [4]. One advantage of this powder based process is the direct accessibility of the ceramic object after printing while parts made from suspensions need to be de-bonded and sintered after the building process [12]. Therefore, powder-based procedures are also called direct fabrication technologies.

Known suspension-based manufacturing procedures are Thermoplastic 3D-Printing (T3DP [13]), Fused Deposition Modeling (FDM [14]), Direct Inkjet-based Printing (also called Direct Ceramic Jet Printing DCJP [15]), extrusion-based direct-writing techniques, light exposure-based lithography technologies such as the Lithography-based Ceramic Manufacturing (LCM) [3,7], and ceramic stereolithography (CSL) [5]. According to Chen et al. [6], the 3D printing of ceramics, LOM as well as FDM, can also be called bulk solid-based technologies to create structural and functional ceramics.

Recently, it has been shown that photopolymerization methods by means of suitable suspension-based slurries represent higher technology potential than powder bed fusion in the manufacturing of 3D ceramics parts or graded porosities features. To name the most promising markets, the photopolymerization technology is used for chemical industries, aerospace, machinery, electronics, micromechanics/microfluidics, piezo-actuators, catalytic surfaces, and photonics and medical industries [6]. In medical technology, a continuous trend to individualization, and thus, to patient-specific implants requires the combination of different properties in one implant component. For that, gradients in functional properties as well as micro- and nano-scaled biomaterial surfaces are favored [16]. However, conventional medical implants such as auditory ossicles, dental implants, finger-, foot-, shoulder-, hip-, or knee implants made from ceramics are still produced by other common techniques that are limited in individual treatment of patients. For medical applications, especially dispersion ceramics like alumina toughened zirconia (ATZ) ceramics as well as ZTA (zirconia toughened alumina) are reliable materials, since they ideally combine a good biocompatibility (inertness) with a high wear resistance, exceptional hardness, high mechanical strength, and slow hydrothermal aging [17–19]. In addition to their outstanding biomechanical properties, the fast and stable ingrowth of host tissue into superficial implant structures is advantageous to inhibit intolerances, hypersensitivities, or allergic reactions, and to promote good osseointegration [20–22]. Crucial for this purpose is the availability of a defined pore gradient as a combination, for example from nano-, micro- and macrostructures which might combine complex microstructures and fine features on the nanoscale [23].

The production of structural-complex ceramic parts requires high resolution and appropriate surface properties to meet the demanding applications. A technique which is particularly suited for the fabrication of patient-individualized, functional, porous 3D structures is direct laser writing via two-photon absorption (TPA) [24]. With TPA, the polymerization is generally initiated by the simultaneous absorption of two photons, usually using near-infrared (780 nm) or green (515 nm) laser light. The photoreaction is initialized by high energy intensity and takes place within a spatially confined focal volume in the corresponding photosensitive resin. It is generally suited to realize free-form 3D shapes with graded porosity in µm- and sub-µm-range in photosensitive materials such as polymers,

hybrid polymers, and composites such as ceramic materials [25–27]. With conventional one-photon-based processes such as CSL [28], this type of three-dimensional structuring, pore size distribution, and resolution is not possible, because the polymerization only takes place at the liquid surface layer. A slurry-based ceramic 3D printing technology like TPA involves liquid or semi-liquid polymer systems with ceramic particles dispersed in the polymer host matrix as feedstock (inks or pastes). Depending on the solid load and the ceramic particle size distribution, opaque ceramic slurries typically used in CSL and DLP processes must be adjusted for TPA processing. In addition, the viscosity of the system resulting from different additives might significantly alter the polymerization kinetics [29,30].

This paper discusses our works to create 3D printed ATZ (alumina toughened zirconia)-like ceramic slurries which are employed to light-induced polymerization by means of TPA to fabricate simple shapes from the µm up to the cm range. Multiple types of photo-curable polymer-ceramic-mixtures of water- and non-water-based slurries for CSL are described and discussed. According to the current DIN standard for the biological evaluation of medical devices, a first experiment to assess the cytocompatibility of TPA-printed ATZ ceramics was carried out and evaluated.

2. Materials and Methods

2.1. Materials

The prepolymer basis used in this study was a solution of acrylamide (AM), methylenebisacrylamide (MBAM), and the dispersant sodium polymethacrylate, which was dissolved in deionized water (all components from Sigma Aldrich GmbH, 97–99% purity). Aluminum oxide (Aerodisp W440, Evonik AG) and zirconium oxide (Zirkonsol, Nanostone GmbH) sols were mixed (pH of the ATZ slurry between 5–6) in a ratio of 20:80 (like an ATZ slurry with 50 wt.%) in a round bottom flask. Subsequently, the solvent was evaporated. As shown in Table 1, the particle size (d_{50}) of the commercially available zirconia sol was between 30 and 35 nm with a particle load of 45 wt.%. The alumina sol (cationically charged) had a particle size (d_{50}) of 110 nm with a particle load of 40 wt.%. As photoinitiator, the commercially available photoinitiator IRGACURE® 2959 (Ciba AG; 2 wt.% based on non-ceramic content) containing polar hydroxyl groups was added to the prepolymer mixture.

Table 1. Commercially available ceramic components used for alumina toughened zirconia. (d_{50} is the mass median diameter which is the portions of particles with diameters smaller and larger than this value are 50%).

	Ceramic	**Producer**	**Particle Size d50 [nm]**	**Particle Load [wt.%]**
Aerodisp W440	Al_2O_3	Evonik	110	40
Zirkonsol	ZrO_2	Nanostone	35	45

The slurry was then stirred for 10 min in order to dissolve agglomerates and to achieve a homogeneous slurry. The rheological behavior was optimized to account for a suitable layer spreading which results in a homogeneous green microstructure. The final viscosity (Modular Compact Rheometer MCR 502, Anton Paar) of the ceramic suspension applied in this experiment was 0.2 mPa·s (value for 100/s, 22 °C). The transmission of the ATZ slurry used for TPA experiments was 40% (value for 522 nm TPA laser wavelength for 500 µm optical path length).

2.2. Methods

2.2.1. TPA Machine

The ATZ like slurry was processed with a commercially available industrial High Precision 3D Lithography Equipment (LithoProf3D®-GSII, Multiphoton Optics GmbH) by

TPA to realize test patterns of 3D structures. The system is based on a femtosecond-pulsed laser working at a laser wavelength of (522 ± 4) nm and a maximum average output power of 650 mW. The system is equipped with a 5-axes system consisting of 3-axes high-precision air-bearing stages and a galvo-scanner system. The laser beam is moved through the liquid ceramic composite material in a synchronized motion. As objectives for the fabrication of 3D structures, either a Zeiss (NA 1.4, ×100) planachromat or a Leica (NA 0.6, ×40) lenses were used.

The objective lens with the highest numerical aperture was used for the highest spatial resolution in a top illumination and a head-first fabrication, i.e., the structures are fabricated head first at the bottom side of the upper glass cover slide (Figure 1a). The objective lens with the lower aperture was also used for fabrication in a top illumination mode where the structures are fabricated at the top side of the lower substrate, i.e., the laser light has to travel through the thick ATZ slurry layers (Figure 1b). The interface was detected with an integrated autofocus system still suited to be used even with these highly particle-loaded slurries. While the fabrication displayed in Figure 1a corresponds to the objective lens design case for the Zeiss planachromat, this is only suited for smaller structures, since the light must travel through the already polymerized structures having a much higher refractive index. This might lead to significant aberrations. It is necessary to focus the laser beam deeper into the ATZ slurry to fabricate larger structures, resulting in a reduction of the fabrication resolution.

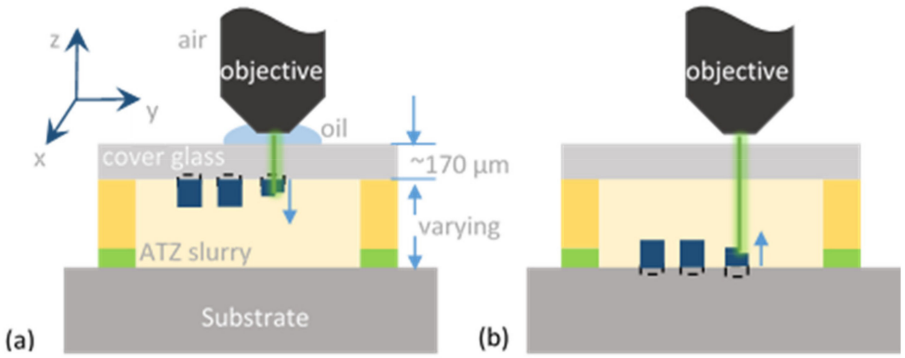

Figure 1. Schematics of the fabrication setups. The material is exposed to the laser light in both setups from the top. (**a**) Head-first fabrication is used for highest resolution and (**b**) structure fabrication at the bottom of the substrate through several hundred microns of ATZ slurry.

2.2.2. Characterization of Test Structures and Biocompatibility Testing

SEM investigations were carried out using a Zeiss Evo LS 10 (Carl Zeiss microscopy GmbH) under high vacuum conditions equipped with an EDX detector Quantax X-flash 3011 (Bruker nano), having an energy resolution of <123 eV. SEM and EDX investigations were carried out at an accelerating voltage of 12 kV at a working distance between 12 and 16 mm. SEM images were taken with a stage tilt angles of 60° to 80°, EDX scans were performed by scanning an area of interest (AOI) of 10 × 10 µm^2 without stage tilt at the center of the structure shown in Section 3.2.

To determine the biocompatibility, a first cytotoxicity test (XTT-assay) according to DIN EN ISO 10993-5: 2009 was carried out with extracts or solutions (indirect cell material contact) of completely processed materials. ATZ ceramic (as used in approved medical products) from the manufacturer Mathys (ATZ-Mathys) as well as ATZ-like structures produced with TPA (ATZ-TPA) were used as test materials. Extracts from both ATZ materials were produced in accordance with the specified DIN, and 0.35 mg/µL were used for production. To prepare the dilution series, 20% of the extracts were further diluted 1:3 over 10 dilution steps. The stock solution was diluted in the same way as negative control. The pre-osteoblast cell line MC3T3 was used as target cells in accordance with the medical application (bone contact). To carry out the biological experiments, 10,000 cells/wells were seeded in a 96-well plate and incubated overnight. Subsequently, the extract was added.

The vitality of the cells was determined with an XTT assay. Usually, XTT is a colorless compound that only becomes detectable at 450 nm after reduction on the surface of an intact cell membrane. In contrast, non-vital cells with a compromised membrane will not reduce the XTT, and hence there is no signal increase at 450 nm.

3. Results and Discussion

3.1. Manufacturing of Ceramic Parts Using Heterogeneous Slurries and Conventional Technologies

CSL processes to produce ceramic parts from water-based slurries were first reported in 1994 by Griffith and Halloran [31] using a 45–55 vol.% water slurry of acrylamide and N,N′-methylene bis-acrylamide (MBAM). They succeeded to produce a green body from the silica-slurry using an UV lamp and a mask with a cure depth of about 300 µm. Two years later, the first fully additively manufactured ceramic piece fabricated with a SLA apparatus and sintered was published also by Griffith and Halloran [32]. Until now, silica and acrylamide/MBAM is the most studied water-based slurry [30]. The refractive index (RI) of the solution is about 1.35–1.50 at 589 nm, which fits to silica ceramic particles with a RI of approximately 1.5. This leads to highly transparent slurries. Additionally, the viscosity is very low, with a value of about 1000 mPa·s, even with highly filled slurries. With such slurries, high curing depths of up to 300 µm and a resolution of 100 µm are possible [33,34]. The inclination angle should not be larger than 30° to reduce delamination and the surface roughness considering the ladder effect [35]. Moreover, other ceramics like alumina [36] or beta tricalcium-phosphate [37] have been produced for scaffolds using an aqueous slurry containing acrylamide/MBAM.

Besides the water-containing slurries, it is also common to use slurries based on organic solutions. The advantage of those is a higher reactivity and the absence of water, which otherwise needs to evaporate during the exothermic UV process. Silica ceramics have a low refractive index of RI589 nm = 1.56 compared to other ceramics. This makes it easier to match with the refractive index of organic binders. For example, sintered silica ceramics [38–41] are produced by using resins containing amorphous silica and low volumetric percentage of as sintering additive (e.g., boron oxide (B2O3)) in hexandioldiacrylate (HDDA), or in a mixture of hydroxyethylmethacrylate (HEMA), tetraethylenglycoldiacrylate (TEGDA) and phenoxyethanol (POE) [42].

Compared to silica, alumina has a higher refractive index of 1.7, which makes it more challenging to find a suitable binder system (e.g., for optical elements). Alumina ceramic parts are widely used in many technologies, and the interest in producing 3D-printed alumina ceramic parts is therefore very high. In 1999, Zhang [36] was the first who showed the fabrication of a ceramic part from HDDA by µ-stereolithography process (µ-SLA) of dense alumina parts with a line width of 1.2 µm. The solid content varied between 40 and 60 wt.% [43–47]. Further used polymers are Acura SI-10 [48] and polyethyleneglycoldiacrylate (PEG-DA) [49]. Buerkle [50] fabricated Dielectric Alumina Resonator Antennas (DRA), which shows that the range of possible applications of additively manufactured alumina ceramic parts is very wide. Using micro photo-forming, Shan [51] reported the fabrication of alumina ceramic parts. Besides HDDA, even barium titanate [52] or piezoelectric PMNT ($0.65Pb(Mg_{1/3}Nb_{2/3})O_3–0.35PbTiO_3$) [53] slurries were used to produce piezoelectric materials (PZT) parts [54–56]. Further, also shown in the literature, quite a variety of slurries used epoxy resins like Adika rascure HS662 to form porcelain parts [57] or SiO_2-TiO_2 to form photonic crystals [58]. Other ceramics produced with SLA were made of $Ba_3ZnTa_2O_9$ (BZT) [59] for RF (radio frequency) devices or aluminum nitride (AlN) [60] for the production of microchannel cold plates. A combination of beta-tricalcium phosphate (β-TCP) and hydroxyapatite (HAP) powder in oligocarbonate-dimethacrylate (OCM-2) can be used to produce implants [61]. Bioactive glass is produced from SOMOS® resin [62] and calcium pyrophosphate (CPP-A) [63] from an acryl polyester resin.

As generally shown from Hannemann et al. [64], the sintering property can be increased by replacing the microscale ceramic particles by nano-sized ceramic particles. CSL is a favorable technique to produce periodic lattices. Duplication of the smallest unit as

CAD model leads to very large objects. Various electrical or optical applications can be addressed by choosing different materials, such as microwave devices [65] from alumina and zirconia, photonic crystals [66,67] or lattices with different refractive indices [68].

Up to now, the synthesis and optimization of heterogeneous slurries on the basis of oxide ceramics or dispersion ceramics, for example on the basis of alumina toughened zirconia (ATZ) by means of TPA, was only rudimentary described [30].

3.2. Structuring of an ATZ like Slurry with TPA

Before TPA experiments started, the general ability of the ATZ slurry to be cross-linked was tested using a commercially available LED light source (365 nm) at a power density of 20 mW/cm^2. In these experiments, isopropanol, ethanol, and deionized water have been proven to be suitable solvents.

Using the TPA equipment from Multiphoton Optics GmbH, a large variety of structuring parameters and methods are accessible and can be screened in a high throughput approach. In order to reduce the possible parameter space to relevant structuring parameters for the specific ATZ slurry, the fabrication parameters, such as the structuring velocity or writing velocity and the applied average laser power, are varied as part of a previously defined parameter search fields.

Cuboids with varying edge length and double pyramids (see designs in Figure 2b,d) were chosen as test structures for the parameter fields. The fabricated cuboids determine shape accuracy by determining edge length and surface flatness and double pyramids show the feasibility of an undercut using ceramic slurries.

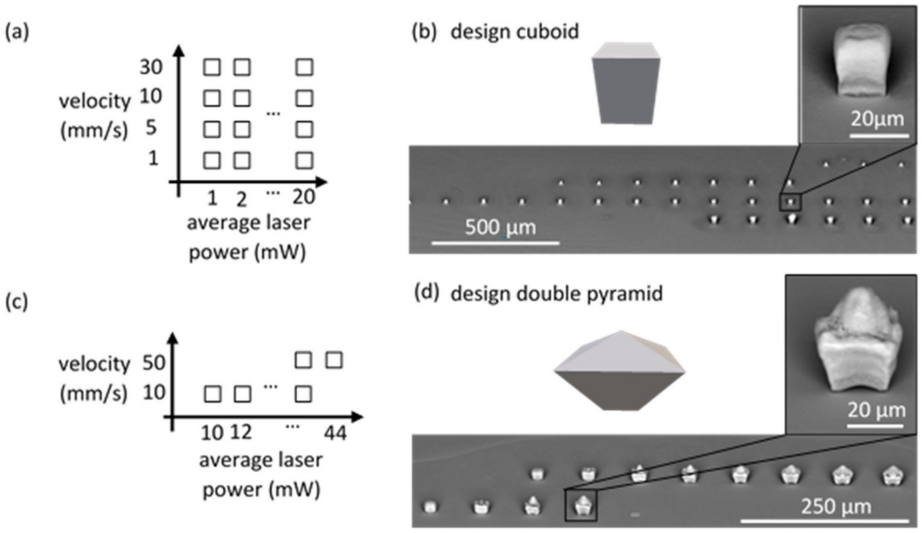

Figure 2. Parameter field for cuboid structures (20 µm × 20 µm × 30 µm). (**a**) Layout (not to scale) and (**b**) overview SEM image with the respective designs. Parameter field for double pyramid structure: (**c**) layout (not to scale) and (**d**) overview SEM image of the structures that remained on the substrate's surface after the development step. Both overview SEM images feature a magnified image of one exemplary structure.

Their designs were imported and further refined in the LithoSoft3D software (Multiphoton Optics GmbH) which enables a fast access to the process parameters. Results of the fabricated structures with corresponding fabrication parameters are displayed in Figure 2 which shows the schematics of a parameter field as well as the default and the fabricated cuboids as investigated by scanning electron microscopy (SEM). The magnified SEM image of the cuboid structure in Figure 2b displays that the fabrication of structures from an ATZ slurry is possible and somewhat accurate. The surface of the structure is not as smooth as for other materials [26,69]. A closer look reveals that the smoothness decreases from bottom to top of the structures. This might be due to non-directed scattering effects resulting from

the ceramic particles incorporated in the polymer host material. Agglomerates of ceramic particles act like point scattering sources increasing and deforming the technical interaction volume. During the fabrication of a structure, the laser beam is moved deeper into the material, resulting in an increasing amount of point scattering sources within the laser beam region. As obvious from the data, shape deviations from the design reveal; in fact, the structure is bigger than the design case, pointing to the fact that more material is polymerized than initially directly exposed in the laser light's focal volume. As already explained by Houbertz et al. [24], there is an enlargement of the light-exposed volume resulting from the polymerization reaction, referred to as chemical interaction volume. This reaction is in contrast to the technical interaction volume based essentially on the IPSF (Intensity Point-Spread Function). The presence of the chemical interaction volume leads to an enlargement of the polymerized structure due to chain reactions and diffusion processes, and these can be further even amplified by non-directed scattering effects. It has to be mentioned, however, that a systematic study of shapes in dependence of the ceramic particle filler content has not yet been carried out, which would reveal the impact on light scattering upon exposure. Although the magnification of the double pyramid structure shows additional shape deviations, structuring of an undercut with TPA in these dispersions ceramic seems feasible.

For the fabrication of these structures, a setup such as displayed in Figure 1a was used. The structuring process in this fabrication mode begins at the bottom side of the cover glass slide, which is in direct contact with the ATZ slurry, and continues from top to bottom along the optical axes into the material volume. The disadvantage of this fabrication mode is that the laser light passes polymerized material for the structure consisting of more than a single layer. In general, polymerized material features different optical properties than unpolymerized material. Therefore, the structuring parameters should be adapted along the structure's height to compensate for effects such as light scattering, aberration, and absorption.

An overview of the parameter space for structuring cuboids (20 µm × 20 µm × 30 µm) using the ATZ slurry is given in Figure 3. Structuring of the ATZ slurry was possible with all chosen structuring velocities up to 50 mm/s with very good results. However, for higher structuring velocities, the average laser power needs to be increased in order to obtain a similar energy dose in the TPA process. The parameter window of this ATZ slurry is much smaller than that of a benchmarking inorganic-organic hybrid polymer of the ORMOCER® material class, which is well suited for 3D structuring by TPA [70,71].

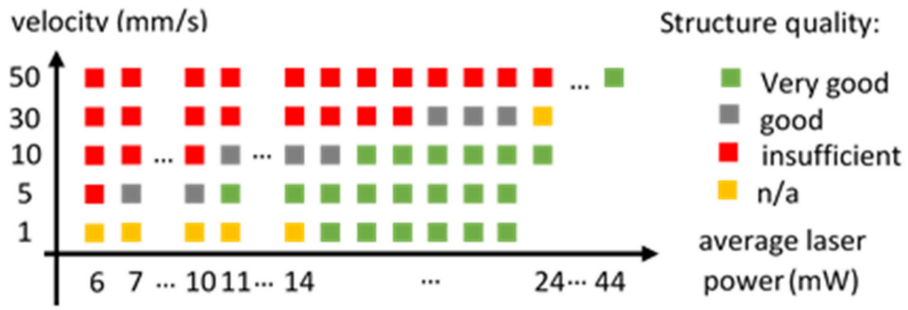

Figure 3. Parameter space for structuring cuboids (20 µm × 20 µm × 30 µm) with TPA using ATZ slurry.

Furthermore, cuboid structures with larger edge length (50 µm × 50 µm × 30 µm) were fabricated alongside of cuboids with similar dimensions as before (20 µm × 20 µm × 30 µm). The structuring results are displayed in Figure 4. While all polymerized small cuboids are attached to the substrate, a notable number of larger structures has delaminated from the substrate's surface during the development step. The shape of the larger cubes (see also the double pyramids in Figure 2) suggests that the ATZ slurry structures experience compressive stress during the fabrication process which was already observed by [72]. The

observation of compressive stresses results from the cross-linking process and it is even enhanced after thermal annealing in the sintering process.

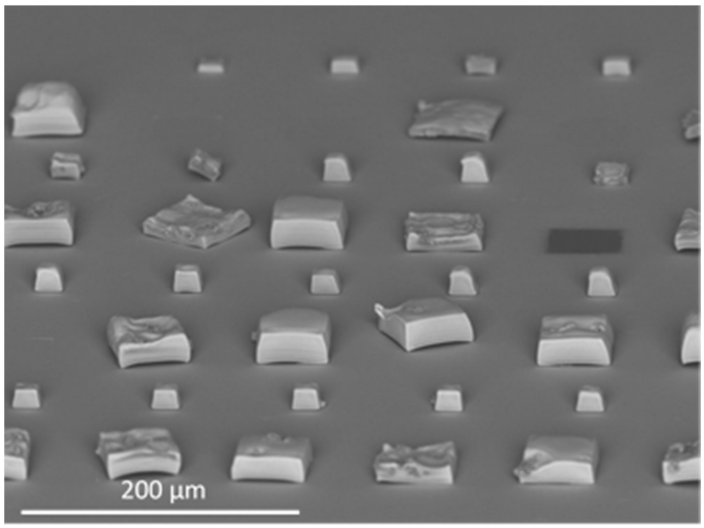

Figure 4. Smaller cuboids (20 µm × 20 µm × 30 µm) and cuboid structures with larger edge length (50 µm × 50 µm × 30 µm), structured with 10 mm/s fabrication velocity and 20 mW average laser power.

Aside of stresses related to the light-induced cross-linking, it is well known that ceramic materials such as composites with a high amount of inorganic content often show crack formation. However, it was demonstrated that materials with an extremely high inorganic content can be structured in 3D by means of TPA without cracking or delamination, which was the result from long-term process parameter optimizations. These resulted either in piezoelectric or ferroelectric layers after thermal annealing [73] or high refractive index materials even without annealing [74].

Further investigations have been carried out to determine whether structuring is possible in deeper material layers. For this purpose, a set-up as in Figure 1b is used. The structure is produced from bottom to top. As mentioned earlier, light adsorption and scattering within the ATZ slurry leads to a power reduction in the focal volume, which can have a significant impact for larger cure depths. In this work, structuring was successfully performed through material layers with material thicknesses up to 480 µm. Figure 5 displays the structuring results through an ATZ material layer of 80 µm thickness. For a lower exposure dose, the 3D structures which were fabricated resemble well the designed structures. However, the structures are deformed if higher exposure doses beyond 35 mW average laser power are used [34]. A closer look at the interface substrate/3D structures shows that below 25 mW compressive stresses play a major role for the delamination process. The structures are at their edges still attached to the substrate and delaminate at their centers. However, between an average laser power of 30–35 mW, the situation seems to be reversed. The edges delaminate and the center adheres to the substrate. For higher average laser power, the structures adhere well to the substrate which is related to an extremely elongated focal volume along the Z axis (optical axis). The lateral extension is less affected by the laser power.

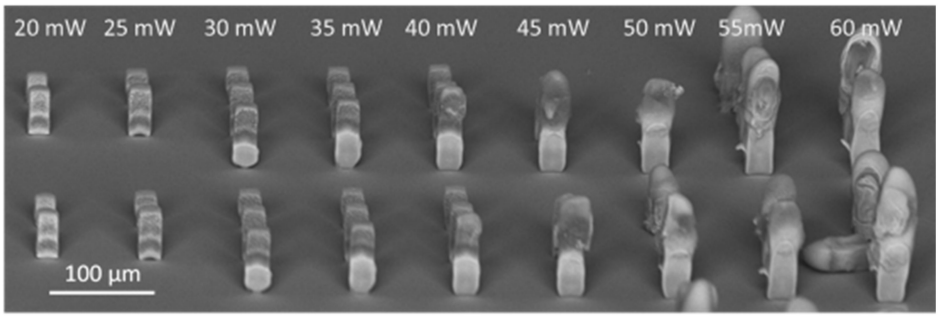

Figure 5. SEM image of structures printed on a glass substrate in a curing depth of 80 µm.

Moreover, one first de-bonding/sintering experiment with a temperature-time-profile commonly used for a standard zirconia oxide ceramic was performed on cuboid structures. It shows that TPA-printed 3D structures can in principle be thermally annealed to create pure ceramic structures. The green structure fabricated by TPA (Figure 6a) was sintered, resulting in compacted ceramic structure (Figure 6b). As shown in Figure 6c, the typical elements for this ATZ ceramic such as Zr, Al, and O were clearly quantified by means of energy dispersive X-ray (EDS) analysis.

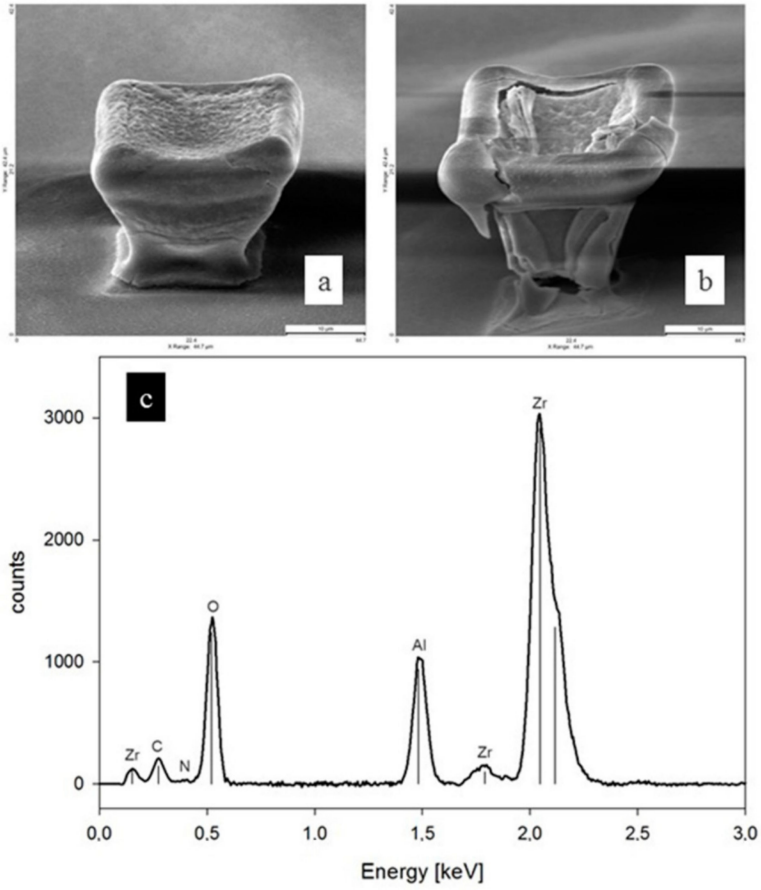

Figure 6. TPA fabricated 3D structure from an ATZ slurry before (**a**) and after (**b**) a non-optimized de-bonding process (scale bar: 10 µm). Elemental composition (EDX analysis (**c**)) after de-bonding shows the main elements of this ATZ ceramic.

Without optimization of the heating process, there are noticeable changes such as, for example (visible) cracks in the de-bonded 3D structure which becomes obvious from Figure 6b. The ceramic structure shrinks more at its bottom, which points to the fact that the laser power (or energy dose) was less than at the top of the structure in the given

setup, resulting in a lower degree of polymerization than at the top of the structure. This was already observed by Stichel et al. [75] who implemented an empirically determined laser power adaptation to overcome the difference in polymerization degree and to create cubic scaffold structures with a homogeneous degree of cross-linking. An iterative optimization of the debonding process which was performed with best results for debonding between 300 and 370 °C to remove the organic binder, followed by a sintering step at 1450 °C resulted in flawless 3D ceramic structures. This shows that an optimization of the temperature-time regime for the debonding and sintering process of the ceramic ATZ sol mixtures [30,33] is essential. The iterative optimization process for debonding and sintering would also prevent pore and crack formation resulting from the fact that all organic/inorganic components from the ATZ slurry (see Section 2.1) are removed during processing.

3.3. Biocompatibility Tests

The biocompatibility testing was performed in a contact free assay according to the DIN EN ISO 10993-5: 2009. The aim was to identify any soluble substance that may influence the cell growth independently from the direct contact to the material, since this may influence the cell behavior itself. Hence, it is easier to estimate if the processing and not the surface characteristic of the material has an impact on the cells. Figure 7 shows that both ATZ materials extracts (indirect cell contact) do not exhibit any cytotoxic effect on cell growth for MC3T3 used in this study. In contrast to the control with dimethyl sulfoxide (DMSO), there is only a slight inhibition of cell growth for some medium dilutions of the extracts from ATZ-TPA. At lower dilutions, DMSO shows as a well described organic solvent expect cytotoxic effects, whereas the effect decreases constantly with higher dilutions. In case of ATZ material extracts, no such correlation between dilution and growth inhibition could be observed. Nevertheless, it seems, that there still exists a slight inhibition of cell growth even at higher dilutions. This is eespecially true for ATZ, which were fabricated by TPA (ATZ-TPA); the growth is obviously hampered in comparison to samples from ATZ Mathys. One explanation might be that the photoinitiator is either not fully eliminated during the development of the ATZ-TPA sample or is not completely removed during de-bonding/sintering. The latter is highly likely because the concentration of photoinitiator in the material exceeds the necessary amount to a certain extent, always leaving unreacted photoinitiator residue in the final material.

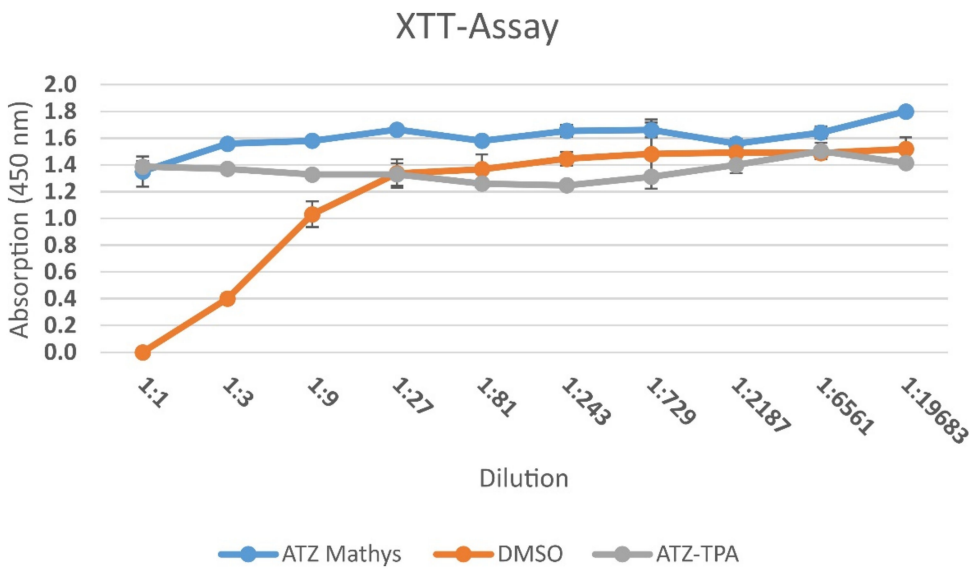

Figure 7. XTT assay of MC3T3 cells for the detection of the cytotoxicity of finished processed material (ATZ-Mathys and ATZ-TPA). Ceramic from Mathys was used as reference material and DMSO as negative control (n = 4 technical replicates).

However, the potential toxicity of the photoinitiator components which are required for photopolymerization on different cells and tissues has not yet been fully addressed [76]. It was demonstrated with other materials such as novel degradable hybrid materials, that the toxic effect of photoinitiators can be completely neglected dependent on the material formulation [77]. Nevertheless, further analysis of experiments using a direct cell-material contact are necessary to thoroughly evaluate the biocompatibility of the produced ceramics. Additionally, for a full quantification of the biocompatibility of TPA-generated structures, more cell lines like, chondrocytes, epithelial cells, and mesenchymal stem cells have to be taken into account. Medical devices are in contact with different cell types, which might react differently to the artificial material.

For the structuring of polymers in the nm to the cm range, the application of TPA is already well established. In contrast, as shown from our results, the transfer of this technique on ceramics has many challenges that need to be solved.

However, scaffolds for cell growth (Figure 8) can be fabricated with TPA with a commercially available hybrid polymer from the ORMOCER® material class. In contrast to such ORMOCER®, heterogeneous ceramic slurries naturally induce scattering of light during the laser processing due to their particulate nature.

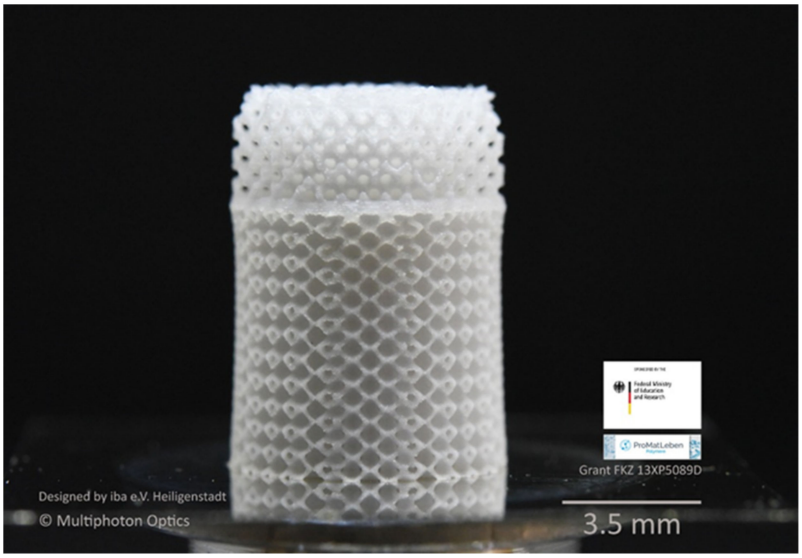

Figure 8. Macroscopic TPA Scaffold made of ORMOCER® (organically modified ceramic) demonstrating the performance of the TPA process as well as the used TPA machine (LithoProf3D®-GSII, Multiphoton Optics GmbH) for producing structured 3D bodies, which is transferred to the novel ATZ materials in the next step.

Consequently, the synthesis of suitable ceramic slurries and their optimization especially for the TPA process plays an important role to enable further ceramic stereolithography (CSL) tools (ongoing process) in the near future to produce graded functionality structures including complex microstructures and fine features. According to that, many investigations have been accomplished in the last decades that deal with the synthesis and characterization of heterogeneous slurries for TPA processing. Ceramic slurries described in the literature are usually particles dispersed in a photocurable resin, which lead to opaque mixtures, thus resulting in a significant challenge for photopolymerization processes. Generally, water-based as well as non-water-based slurries have been investigated regarding their suitability for the production of ceramic 3D structures using CLS [4,6].

4. Conclusions

In conclusion, basic aspects of the photo-chemical micro- and nano-lithography using TPA for ceramic slurries as shown in this paper on three dimensional objects like cuboids and pyramids in the µm-range could be clarified by means of the experiments described in

this paper. For the first time, it was demonstrated that heterogeneous ATZ-based ceramic slurries can be structured using TPA in a standard fabrication mode [23,78]. Therefore, our work has made an important contribution to the development of photochemical microlithography by means of TPA for the preparation of oxide ceramic (as shown for ATZ) 3D structures. This will help to exploit the high potential of TPA in the field of 3D structuring of various oxide ceramic suspensions/slurries in the near future.

It still needs to be considered, that—as with gel casting—the green body density of the TPA-formed structure is determined by the ceramic volume fraction in the suspension. For adequate de-bonding/sintering behavior, the green density and thus the suspension volume fraction must be approximately 50 vol.% or higher. For this reason, a key feature of ceramic technologies involving photopolymerization is to achieve the proper rheology of highly loaded suspension.

Moreover, this work states that the TPA technique can be used for the additive fabrication of ceramic 3D structures, while for larger structures (>480 µm in height and >50 µm × 50 µm base area) a redesign of the setup is recommended. Nevertheless, this technique must ensure a finer layering than for example Large Area Maskless Photopolymerization (LAMP) to create a real micro resolution in all three dimensions. Moreover, it is extremely useful to understand how parameters (cure depth and energy dose) depend on the composition of the suspension, the used photoinitiators and dyes, and the physicochemical and optical nature and amount of the used ceramic powder. For the last point, the response function of the material formulation to the laser light can be used to find out the restrictions of the structuring resolution.

In order to produce ceramic microscale components with high precision and graded mechanical or topographic properties in the future, supplementary investigations are necessary. It would be important to study the swelling and shrinking of the structures during the fabrication and sinter process. Furthermore, the technical and chemical interaction volume as well as the threshold behavior need to be intensively studied to understand the light-matter interaction of highly ceramic particle loaded material systems. Another key requirement on a reliable material is the processing and long-term stability that requires further attention. The conventional way to additively manufacture large structures is to split the given design file into slices and hatches. Depending on the slice and hatch spacing, this approximation of the design file can lead to long writing times. If the distances are increased, the writing time decreases, whereby the structure quality and the dimensional accuracy naturally deteriorate. If the processed ceramic slip is sufficiently stable after crosslinking, it may be possible to write only the shell of the given structure with TPA. After the necessary development step, the still liquid inner material can be cross-linked, e.g., by a flat UV exposure. The stability of the shell must be adjusted depending on the size and shape of the object. With this procedure, it is possible to reduce the writing times drastically or to produce small 3D parts.

5. Patents

Offenlegungsschrift (4 January 2018, patent examination via "Deutsches Patent-und Markenamt" still under progress): DE 10 2017 205 432 A1: Herstellung von Keramikstrukturen mittels Mehrphotonenpolymerisation.

Author Contributions: Conceptualization, G.H. and K.L.; methodology, U.S., J.C.S., W.M., Y.D. and R.H.; file preparation for TPA processing, W.M. and Y.D.; formal analysis, U.S.; investigation, J.C.S., U.S., W.M. and Y.D.; resources, J.C.S., U.S., W.M., Y.D.; writing—original draft preparation, G.H., J.C.S., U.S., W.M. and Y.D.; writing—review and editing, G.H., R.H. Support in TPA processing of slurries; R.H. and K.L.; supervision, R.H. and K.L.; project administration, K.L. and R.H.; funding acquisition, G.H. and K.L. All authors have read and agreed to the published version of the manuscript.

Funding: The financial support from the "Thüringer Ministerium für Wirtschaft, Wissenschaft und Digitale Gesellschaft (TMWWDG)" under Grant Number 2015 FE 9117 (co-financed from EFRE) as well as the "Bundesministerium für Bildung und Forschung" (grant number: 13XP5089C and 13XP5089D) is gratefully acknowledged.

Institutional Review Board Statement: Not applicable.

Informed Consent Statement: Not applicable.

Data Availability Statement: All data are stored in an electronic laboratory book.

Acknowledgments: We would like to thank Mathys Orthopädie GmbH (Mörsdorf, Germany) for providing the ATZ samples as reference material for biological tests.

Conflicts of Interest: The authors declare no conflict of interest.

References

1. Doreau, F.; Chaput, C.; Chartier, T. Stereolithography for Manufacturing Ceramic Parts. *Adv. Eng. Mater.* **2000**, *2*, 493–496. [CrossRef]
2. Moritz, T.; Partsch, U.; Ziesche, S.; Scheithauer, U.; Ahlhelm, M.; Schwarzer, E.; Richter, H.-J. *Additive Fertigung von Keramik*; Jahresbericht 2014/2015; Fraunhofer IKTS: Hermsdorf, Germany, 2015; pp. 28–31.
3. Zocca, A.; Colombo, P.; Gomes, C.M.; Günster, J. Additive Manufacturing of Ceramics: Issues, Potentialities, and Opportunities. *J. Am. Ceram. Soc.* **2015**, *98*, 1983–2001. [CrossRef]
4. Deckers, J.; Vleugels, J.; Kruth, J.-P. Additive manufacturing of ceramics: A review. *J. Ceram. Sci. Technol.* **2014**, *5*, 245–260.
5. Halloran, J.W. Ceramic Stereolithography: Additive Manufacturing for Ceramics by Photopolymerization. *Annu. Rev. Mater. Res.* **2016**, *46*, 19–40. [CrossRef]
6. Chen, Z.; Li, Z.; Li, J.; Liu, C.; Lao, C.; Fu, Y.; Liu, C.; Li, Y.; Wang, P.; Yi, H. 3D printing of ceramics: A review. *J. Eur. Ceram. Soc.* **2019**, *39*, 661–687. [CrossRef]
7. Schwarzer, E.; Holtzhausen, S.; Scheithauer, U.; Ortmann, C.; Oberbach, T.; Moritz, T.; Michaelis, A. Process development for additive manufacturing of functionally graded alumina toughened zirconia components intended for medical implant application. *J. Eur. Ceram. Soc.* **2018**. [CrossRef]
8. Mudge, R.P.; Wald, N.R. Laser engineered net shaping advances additive manufacturing and repair. *Weld. J.* **2007**, *86*, 44.
9. Balla, V.K.; Bose, S.; Bandyopadhyay, A. Processing of Bulk Alumina Ceramics Using Laser Engineered Net Shaping. *Int. J. Appl. Ceram. Technol.* **2008**, *5*, 234–242. [CrossRef]
10. Sing, S.L.; Yeong, W.Y.; Wiria, F.E.; Tay, B.Y.; Zhao, Z.; Thao, L.; Tian, T.; Yang, S. Direct selective laser sintering and melting of ceramics. a review. *Rapid Prototyp. J.* **2017**, *23*, 611–623. [CrossRef]
11. Zhang, Y.; He, X.; Du, S.; Zhang, J. Al_2O_3 Ceramics Preparation by LOM (Laminated Object Manufacturing). *Int. J. Adv. Manuf. Technol.* **2001**, *17*, 531–534. [CrossRef]
12. Schwentenwein, M.; Homa, J. Additive Manufacturing of Dense Alumina Ceramics. *Int. J. Appl. Ceram. Technol.* **2015**, *12*, 1–7. [CrossRef]
13. Cima, M.J.; Sachs, E.M. Three dimensional printing: Forms, materials and performance. In *1991 International Solid Freeform Fabrication Symposium*; Massachusetts Institute of Technology, Department of Materials Science and Mechanical Engineering: Cambridge, MA, USA, 1991; pp. 187–194.
14. Kalita, S.J.; Bose, S.; Hosick, H.L.; Bandyopadhyay, A. Development of controlled porosity polymer-ceramic composite scaffolds via fused deposition modeling. *Mater. Sci. Eng. C* **2003**, *23*, 611–620. [CrossRef]
15. Sirringhaus, H.; Shimoda, T. Inkjet printing of functional materials. *MRS Bull.* **2003**, *28*, 802–806. [CrossRef]
16. Bruinink, A.; Bitar, M.; Pleskova, M.; Wick, P.; Krug, H.F.; Maniura-Weber, K. Addition of nanoscaled bioinspired surface features: A revolution for bone related implants and scaffolds? *J. Biomed. Mater. Res. A* **2014**, *102*, 275–294. [CrossRef]
17. Al-Hajjar, M. Wear of novel ceramic-on-ceramicbearings under adverse ans clinically relevant hip simulator conditions. *J. Biomed. Mater. Res. Part B Appl. Biomater.* **2013**, *101*, 1456–1462. [CrossRef]
18. Oberbach, T. Current state and future trends in bioceramics for orthopaedic applications. In Proceedings of the Global Roadmap for Ceramics—ICC, International Congress on Ceramics, Verona, Italy, 1 September 2008.
19. Begand, S.; Oberbach, T.; Glien, W. ATZ—A new material with high Potential in Joint Replacement. *Key Eng. Mater.* **2005**, *284–286*, 983–986. [CrossRef]
20. Razzante, M.C.; Ehredt, D.J.; Clougherty, C.O.; Kriger, S.J.; Menninger, B.A.; Behan Dionisopoulos, S.; Bhakta, P.J.; Bruning, N.G. Type IV Cell-Mediated Hypersensitivity Reaction Caused by Titanium Implant Following Double Calcaneal Osteotomy and First Metatarsal-Cuneiform Arthrodesis: A Case Report and Review of the Literature. *J. Foot Ankle Surg.* **2019**, *58*, 974–979. [CrossRef]
21. Hofmann, S.C.; Plett, M.; Jansen, S.; Thomas, P.; Tholken, K.F.M. Titanium hypersensitivity causing painful intra-abdominal oedema after staple-fixed inguinal hernia repair. *Contact Dermat.* **2018**, *79*, 48–49. [CrossRef]

22. Thomas, P.; Bandl, W.D.; Maier, S.; Summer, B.; Przybilla, B. Hypersensitivity to titanium osteosynthesis with impaired fracture healing, eczema, and T-cell hyperresponsiveness in vitro: Case report and review of the literature. *Contact Dermat.* **2006**, *55*, 199–202. [CrossRef]
23. Oberbach, T.; Ortmann, C.; Müller, J.C.; Hildebrand, G.; Liefeith, K. Herstellung von Keramikstrukturen Mittels Mehr-Photonenpolymerisation. German Patent No.: DE102017205432, 1 April 2018.
24. Houbertz, R.; Steenhusen, S.; Stichel, T.; Sextl, G. Two-Photon Polymerization of Inorganic-Organic Hybrid Polymers as Scalable Technology Using Ultra-Short Laser Pulses. In *Coherence and Ultrashort Pulse Laser Emission Source*; InTech: London, UK, 2010. [CrossRef]
25. Doraiswamy, A.; Patz, T.; Narayan, R.J.; Chichkov, B.; Ovsianikov, A.; Houbertz, R.; Chrisey, D.B. Biocompatibility of CAD/CAM ORMOCER polymer scaffold structures. *MRS Proc.* **2004**, *845*. [CrossRef]
26. Stichel, T.; Hecht, B.; Houbertz, R.; Sextl, G. Two-photon Polymerization as Method for the Fabrication of Large Scale Biomedical Scaffold Applications. *JLMN J. Laser Micro Nanoeng.* **2010**, *5*. [CrossRef]
27. Burmeister, F.; Steenhusen, S.; Houbertz, R.; Asche, T.S.; Nickel, J.; Nolte, S.; Tucher, N.; Tünnermann, A.; Walles, H. Two-photon polymerization of inorganic-organic polymers for biomedical and microoptical applications. In *Optically Induced Nanostructures*; Ostendorf, A., König, K., Eds.; De Gruyter: Berlin, Germany, 2015; pp. 239–265.
28. Chapute, C.; Chartier, T. Fabrication of ceramics by stereolithography. Rapid Prototyp. 4 Ausgabe 2007. Available online: www.rtejournal.de (accessed on 7 March 2021).
29. Platte, D. Grenzflächenselektive Verkapselung von anorganischen Latentwärmespeicher-Materialien mit Hybridpoylmeren. Ph.D. Thesis, Julius Maximilian University Würzburg, Würzburg, Germany, 2012.
30. Sänger, J.C.; Pauw, B.R.; Sturm, H.; Günster, J. First time additively manufactured advanced ceramics by using two-photon polymerization for powder processing. *Open Ceram.* **2020**, *4*, 100040. [CrossRef]
31. Griffith, M.L.; Halloran, J.W. Ultraviolet curing of highly loaded ceramic suspensions for stereolithography of ceramics. In *Proceedings Solid Freeform Fabrication Symposium*; 1994; pp. 396–403. Available online: http://hdl.handle.net/2152/68676 (accessed on 7 March 2021).
32. Griffith, M.L.; Halloran, J.W. Freeform Fabrication of Ceramics via Stereolithography. *J. Am. Ceram. Soc.* **1996**, *79*, 2601–2608. [CrossRef]
33. Zhou, W.; Li, D.; Wang, H. A novel aqueous ceramic suspension for ceramic stereolithography. *Rapid Prototyp. J.* **2010**, *16*, 29–35. [CrossRef]
34. Chen, Z.; Li, D.; Zhou, W.; Wang, L. Curing characteristics of ceramic stereolithography for an aqueous-based silica suspension. *Proc. Inst. Mech. Eng. Part B J. Eng. Manuf.* **2010**, *224*, 641–651. [CrossRef]
35. Tian, X.; Li, D.; Chen, Z.; Zhou, W. Study on the fabrication accuracy of ceramic parts by direct stereolithography. *Virtual Phys. Prototyp.* **2012**, *7*, 195–202. [CrossRef]
36. Zhang, X.; Jiang, X.N.; Sun, C. Micro-stereolithography of polymeric and ceramic microstructures. *Sens. Actuators A Phys.* **1999**, *77*, 149–156. [CrossRef]
37. Weiguo, B.; Dichen, L.; Qin, L.; Weijie, Z.; Linzhong, Z.; Xiang, L.; Zhongmin, J. Design and fabrication of a novel porous implant with pre-set channels based on ceramic stereolithography for vascular implantation. *Biofabrication* **2011**, *3*, 034103.
38. Corcione, C.E.; Greco, A.; Montagna, F.; Licciulli, A.; Maffezzoli, A. Silica moulds built by stereolithography. *J. Mater. Sci.* **2005**, *40*, 4899–4904. [CrossRef]
39. Corcione, C.E.; Montagna, F.; Greco, A.; Licciulli, A.; Maffezzoli, A. Free form fabrication of silica moulds for aluminium casting by stereolithography. *Rapid Prototyp. J.* **2006**, *12*, 184–188. [CrossRef]
40. Bae, C.-J.; Halloran, J.W. Integrally Cored Ceramic Mold Fabricated by Ceramic Stereolithography. *Int. J. Appl. Ceram. Technol.* **2011**, *8*, 1255–1262. [CrossRef]
41. Bae, C.J.; Halloran, J.W. Influence of Residual Monomer on Cracking in Ceramics Fabricated by Stereolithography. *Int. J. Appl. Ceram. Technol.* **2011**, *8*, 1289–1295. [CrossRef]
42. Kotz, F.; Arnold, K.; Bauer, W.; Schild, D.; Keller, N.; Sachsenheimer, K.; Nargang, T.M.; Richter, C.; Helmer, D.; Rapp, B.E. Three-dimensional printing of transparent fused silica glass. *Nature* **2017**, *544*, 337–339. [CrossRef]
43. Hinczewski, C.; Corbel, S.; Chartier, T. Ceramic suspensions suitable for stereolithography. *J. Eur. Ceram. Soc.* **1998**, *18*, 583–590. [CrossRef]
44. Hinczewski, C.; Corbel, S.; Chartier, T. Stereolithography for the fabrication of ceramic three dimensional parts. *Rapid Prototyp. J.* **1998**, *4*, 104–111. [CrossRef]
45. Chartier, T.; Chaput, C.; Doreau, F.; Loiseau, M. Stereolithography of structural complex ceramic parts. *J. Mater. Sci.* **2002**, *37*, 3141–3147. [CrossRef]
46. Goswami, A.; Ankit, K.; Balashanmugam, N.; Umarji, A.M.; Madras, G. Optimization of rheological properties of photopolymerizable alumina suspensions for ceramic microstereolithography. *Ceram. Int.* **2014**, *40*, 3655–3665. [CrossRef]
47. Adake, C.V.; Gandhi, P.; Bhargava, P. Fabrication of Ceramic Component Using Constrained Surface Microstereolithography. *Procedia Mater. Sci.* **2014**, *5*, 355–361. [CrossRef]
48. Wang, J.-C. A novel fabrication method of high strength alumina ceramic parts based on solvent-based slurry stereolithography and sintering. *Int. J. Precis. Eng. Manuf.* **2013**, *14*, 485–491. [CrossRef]

49. Bertsch, A.; Sébastien, J.; Philippe, R. Microfabrication of ceramic components by microstereolithography. *J. Micromech. Microeng.* **2004**, *14*, 197. [CrossRef]
50. Buerkle, A.; Brakora, K.F.; Sarabandi, K. Fabrication of a DRA Array Using Ceramic Stereolithography. *IEEE Antennas Wirel. Propag. Lett.* **2006**, *5*, 479–482. [CrossRef]
51. Shan, X.; Takagi, T.; Yanagisawa, K.; Nakajima, N. Development of a Manufacturing Process for Ceramic Microstructures by Using Micro Photoforming (1st Report)-Principle of the Process and Photoforming Experiment. *J. Jpn. Soc. Precis. Eng.* **1995**, *61*, 420. [CrossRef]
52. Jang, J.H.; Wang, S.; Pilgrim, S.M.; Schulze, W.A. Preparation and Characterization of Barium Titanate Suspensions for Stereolithography. *J. Am. Ceram. Soc.* **2000**, *83*, 1804–1806. [CrossRef]
53. Woodward, D.I.; Purssell, C.P.; Billson, D.R.; Hutchins, D.A.; Leigh, S.J. Additively-manufactured piezoelectric devices. *Phys. Status Solidi* **2015**, *212*, 2107–2113. [CrossRef]
54. Sun, C.; Zhang, X. Experimental and numerical investigations on microstereolithography of ceramics. *J. Appl. Phys.* **2002**, *92*, 4796–4802. [CrossRef]
55. Sun, C.; Zhang, X. The influences of the material properties on ceramic micro-stereolithography. *Sens. Actuators A Phys.* **2002**, *101*, 364–370. [CrossRef]
56. Kwok, K.W.; Chan, H.L.W.; Choy, C.L. Evaluation of the material parameters of piezoelectric materials by various methods. *IEEE Trans. Ultrason. Ferroelectr. Freq. Control* **1997**, *44*, 733–742. [CrossRef]
57. Satoh, N.; Ueda, Y.; Yorimoto, T.; Aita, H.; Matsuo, S.; Ohata, N.; Watari, F. Firing Shrinkage of Porcelain-resin Composites Prepared by Laser Lithography. *Dent. Mater. J.* **1999**, *18*, 444–452. [CrossRef]
58. Mori, H.; Kirihara, S.; Miyamoto, Y. Fabrication of three-dimensional ceramic photonic crystals and their electromagnetic properties. *J. Eur. Ceram. Soc.* **2006**, *26*, 2195–2198. [CrossRef]
59. Delhote, N.; Baillargeat, D.; Verdeyme, S.; Delage, C.; Chaput, C. Ceramic Layer-By-Layer Stereolithography for the Manufacturing of 3-D Millimeter-Wave Filters. *IEEE Trans. Microw. Theory Tech.* **2007**, *55*, 548–554. [CrossRef]
60. Jankowski, N.R.; Everhart, L.; Geil, B.R.; Tipton, C.W.; Chaney, J.; Heil, T.; Zimbeck, W. Stereolithographically fabricated aluminum nitride microchannel substrates for integrated power electronics cooling. In Proceedings of the 2008 11th Intersociety Conference on Thermal and Thermomechanical Phenomena in Electronic Systems, Orlando, FL, USA, 28–31 May 2008; pp. 180–188.
61. Popov, V.K.; Evseev, A.V.; Ivanov, A.L.; Roginski, V.V.; Volozhin, A.I.; Howdle, S.M. Laser stereolithography and supercritical fluid processing for custom-designed implant fabrication. *J. Mater. Sci. Mater. Med.* **2004**, *15*, 123–128. [CrossRef] [PubMed]
62. Li, Z.; Chen, X.; Zhao, N.; Dong, H.; Li, Y.; Lin, C. Stiff macro-porous bioactive glass–ceramic scaffold: Fabrication by rapid prototyping template, characterization and in vitro bioactivity. *Mater. Chem. Phys.* **2013**, *141*, 76–80. [CrossRef]
63. Talib, M.; Covington, J.A.; Bolarinwa, A. Characterization of Fabricated Three Dimensional Scaffolds of Bioceramic-Polymer Composite via Microstereolithography Technique. *AIP Conf. Proc.* **2014**, *1584*, 129–135. [CrossRef]
64. Hanemann, T.; Boehm, J.; Henzi, P.; Honnef, K.; Litfin, K.; Ritzhaupt-Kleissl, E.; Hausselt, J. From micro to nano: Properties and potential applications of micro- and nano-filled polymer ceramic composites in microsystem technology. *IEE Proc. Nanobiotechnol.* **2004**, *151*, 167–172. [CrossRef]
65. Chartier, T.; Duterte, C.; Delhote, N.; Baillargeat, D.; Verdeyme, S.; Delage, C.; Chaput, C. Fabrication of Millimeter Wave Components Via Ceramic Stereo- and Microstereolithography Processes. *J. Am. Ceram. Soc.* **2008**, *91*, 2469–2474. [CrossRef]
66. Kirihara, S.; Niki, T. Three-Dimensional Stereolithography of Alumina Photonic Crystals for Terahertz Wave Localization. *Int. J. Appl. Ceram. Technol.* **2015**, *12*, 32–37. [CrossRef]
67. Chen, S.; Li, D.; Tian, X.; Wang, M.; Dai, W. Effective fabrication method of 3D ceramic photonic crystals with diamond structure. *Rapid Prototyp. J.* **2012**, *18*, 49–55. [CrossRef]
68. Brakora, K.F.; Halloran, J.; Sarabandi, K. Design of 3-D Monolithic MMW Antennas Using Ceramic Stereolithography. *IEEE Trans. Antennas Propag.* **2007**, *55*, 790–797. [CrossRef]
69. Stender, B.; Hilbert, F.; Dupuis, Y.; Krupp, A.; Mantei, W.; Houbertz, R. Manufacturing strategies for scalable high-precision 3D printing of structures from the micro to macro range. *Adv. Opt. Technol.* **2019**, *8*, 225–231. [CrossRef]
70. Serbin, J.; Egbert, A.; Ostendorf, A.; Chichkov, B.N.; Houbertz, R.; Domann, G.; Schulz, J.; Cronauer, C.; Fröhlich, L.; Popall, M. Femtosecond laser-induced two-photon polymerization of inorganic–organic hybrid materials for applications in photonics. *Opt. Lett.* **2003**, *28*, 301–303. [CrossRef]
71. Houbertz, R.; Schulz, J.; Serbin, J.; Chichkov, B. Schnelle Herstellung photonischer Kristalle: Echtzeit-3D-Lithographie mit Hybridpolymeren. *Phys. Unserer Zeit* **2005**, *36*, 278–285. [CrossRef]
72. Farsari, M.; Filippidis, G.; Fotakis, C. Fabrication of three-dimensional structures by three-photon polymerization. *Opt. Lett.* **2005**, *30*, 3180–3182. [CrossRef]
73. Collin, D. Untersuchungen zu photostrukturierbaren piezo- und ferroelektrischen Dünnschichten. Ph.D. Thesis, Julius Maximilian University Würzburg, Würzburg, Germany, 2014.
74. Houbertz, R.; Declerck, P.; Passinger, S.; Ovsianikov, A.; Serbin, J.; Chichkov, B. Investigations on the generation of photonic crystals using two-photon polymerization (2PP) of inorganic-organic hybrid polymers with ultra-short laser pulses. *Phys. Status Solidi* **2007**, *204*, 3662–3675. [CrossRef]

75. Stichel, T.; Hecht, B.; Houbertz, R.; Sextl, G. Compensation of spherical aberration influences for two-photon polymerization patterning of large 3D scaffolds. *Appl. Phys. A Mater.* **2015**, *121*, 187–191. [CrossRef]
76. Williams, C.G.; Malik, A.N.; Kim, T.K.; Manson, P.N.; Elisseeff, J.H. Variable cytocompatibility of six cell lines with photoinitiators used for polymerizing hydrogels and cell encapsulation. *Biomaterials* **2005**, *26*, 1211–1218. [CrossRef] [PubMed]
77. Obel, K.; Steenhusen, S.; Hümmer, J.; Jurado, G.; Wolter, H.; Houbertz, R.; Nique, S.; Sextl, G.; Walles, H. Novel partially degradable hybrid polymers for biomedical applications. In Proceedings of the 3rd European Symposium of Photopolymer Science, Wien, Austria, 9–12 September 2014.
78. Hildebrand, G.; Müller, J.C.; Rost, J.; Liefeith, K. *Zwei-Photonen-Polymerisation zur Additiven Fertigung von Keramiken. Abschlussbericht des iba Heiligenstadt zum Verbundvorhaben 2015 VF 0041 bzw. iba Teilprojekt (2015 FE 9117) im Rahmen der Richtlinie zur Förderung von Forschung, Technologie und Innovation (FTI) des Freistaats Thüringen*; Thüringer Aufbaubank: Erfurt, Germany, 2019; pp. 1–54.